IEICE TRANS. COMMUN., VOL.E85–B, NO.12 DECEMBER 2002

PAPER

Correction of Numerical Phase Velocity Errors in Nonuniform FDTD Meshes

Andreas CHRIST[†], **Jürg FRÖHLICH**[††], *and* **Niels KUSTER**[††], ***Nonmembers***

SUMMARY This paper proposes a novel method to correct numerical phase velocity errors in FDTD meshes with nonuniform step size. It enables the complete compensation of the phase velocity errors introduced by the mesh grading for one frequency and one arbitrary direction of propagation independently of the mesh grading. This permits the usage of the Total-Field-Scattered-Field formulation in connection with electrically large nonuniform FDTD meshes and allows a general reduction of the grid dispersion errors. The capabilities of the proposed method are demonstrated with the help of two examples: (1) the fields in a dielectric sphere illuminated by a plane wave are calculated and (2) a patch antenna simulation demonstrates that the uncertainty in determining its resonance frequency can be reduced by about 50%.

key words: *nonuniform FDTD, numerical dispersion, total-field scattered-field*

1. Introduction

The finite-difference time-domain (FDTD) method has proven to be a robust and flexible technique for the solution of various kinds of problems in electromagnetics. Originally formulated by Yee [1] in 1966, it has gained increased interest among major researchers during the last decades [2]–[4], developing it into one of the most preferred methods for the solution of complex electromagnetic problems [5]–[7]. The FDTD algorithm uses a central-difference scheme of Maxwell's equations and can therefore yield solutions of second order accuracy. However, this central difference scheme requires the use of equidistant mesh steps, which renders the correct modeling of structures with fine geometrical details infeasible or at least computationally expensive. One common resort to this problem is to use nonuniform mesh steps.

The drawback of nonuniform FDTD meshes is the loss of the central difference and therefore of the second order accuracy. Although the algorithm retains its global second order convergence, as shown in [8], local first order errors do influence the simulation outcome, depending on the cell size and grading ratio. Nevertheless, various studies have shown that the savings in computational power clearly outweigh the impact of the grading on the accuracy of the results [9]–[11]. Other authors [12], [13] have heuristically derived rules for the mesh generation to keep the local error introduced by the grading within certain limits.

In addition, several suggestions have been made to further reduce or overcome the errors in nonuniform meshes (See, e.g., [14], [15]). In all these suggestions, one or two additional field components are incorporated into those finite-difference equations which lose their central-difference characteristics because of the irregular cell spacing. In order to improve the characteristics of the algorithm, the authors introduce different weighting coefficients for these field components. An overview of these methods and their efficiency can be found in [15].

One of the main error sources in the FDTD algorithm is numerical dispersion. Dispersion errors have been thoroughly studied for uniform meshes, and a detailed analysis can be found in [16]. The authors of [17], [18] and [19] suggest modifying the material coefficients in order to reduce the average dispersion error in the grid. This method, however, can efficiently be used only with equidistantly spaced meshes.

In [20] an approach is made to describe the influence of the mesh grading on the dispersion error. The authors derive an expression for the numerical propagation constant in nonuniform meshes from the dispersion relation of the uniform FDTD algorithm.

This paper presents a more rigorous way to derive the numerical phase velocity based directly on the update equations of the nonuniform FDTD algorithm. Thereby, it is shown that the grading of the mesh leads to a complex numerical wave number causing spurious amplification or attenuation. In order to reduce these additional errors, a novel method is proposed by which the accuracy of the original second order central-difference scheme can be fully recovered for a particular frequency and propagation direction. Furthermore, this enables the application of the Total-Field-Scattered-Field formulation [21] on electrically large scatterers in nonuniform meshes.

The remainder of this paper is divided into four major sections. First, the dispersion effects in nonuniform meshes are analyzed in one dimension. The next section introduces and discusses the phase velocity correction. The third section deals with its extension to three dimensions. Eventually, the performance of the novel method is demonstrated with the help of two ex-

Manuscript received March 27, 2002.
Manuscript revised June 10, 2002.

[†]The author is with the Integrated Systems Laboratory, ETH, Zürich, Switzerland.
[††]The authors are with the Foundation for Research on Information Technologies in Society, Zürich, Switzerland.

amples: a dielectric sphere illuminated by a plane wave, and the feedpoint impedance calculation of a patch antenna. In order to keep the paper self-contained, the basic dispersion properties of the FDTD algorithm are briefly reviewed within the bounds of the corresponding sections.

2. Numerical Dispersion in Nonuniform FDTD Meshes in One Dimension

In addition to the dispersion errors of the uniform FDTD algorithm, two different effects increase the numerical phase distortion in the nonuniform mesh: First of all, the loss of the central difference reduces the accuracy of the finite-difference equations. Secondly, the majority of the mesh cells is updated with a Courant factor of less than 1, because the time step must be chosen according to the size of the smallest cell. Since these mechanisms are the same for the one-dimensional and the three-dimensional formulations of the FDTD algorithm, this section focuses on the analysis of the numerical dispersion in one-dimensional nonuniform meshes.

2.1 Nonuniform Dispersion Equation

For staggered nonuniform meshes as in Fig. 1, the FDTD update equations can be written as

$$E|_i^{n+1} = ca_i\, E|_i^n + cb_i\, \left(H|_{i+\frac{1}{2}}^{n+\frac{1}{2}} - H|_{i-\frac{1}{2}}^{n+\frac{1}{2}}\right) \tag{1}$$

and

$$H|_{i+\frac{1}{2}}^{n+\frac{1}{2}} = da_i\, H|_{i+\frac{1}{2}}^{n-\frac{1}{2}} + db_i\, (E|_{i+1}^n - E|_i^n) \tag{2}$$

with the update coefficients

$$ca_i = \frac{2\,\epsilon - \sigma\,\Delta t}{2\,\epsilon + \sigma\,\Delta t} \tag{3}$$

$$cb_i = -\frac{4\,\Delta t}{(\Delta x_i + \Delta x_{i-1})\,(2\,\epsilon + \sigma\,\Delta t)} \tag{4}$$

$$da_i = \frac{2\,\mu - \rho\,\Delta t}{2\,\mu + \rho\,\Delta t} \tag{5}$$

$$db_i = -\frac{2\,\Delta t}{\Delta x_i\,(2\,\mu + \rho\,\Delta t)}. \tag{6}$$

In Eqs. (5) and (6), ρ represents the magnetic losses. For this formulation of the Yee-algorithm, only the accuracy of Eq. (1) reduces to first order, whereas Eq. (2) retains its central difference.

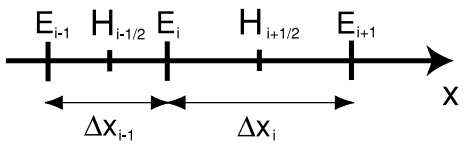

Fig. 1 One-dimensional nonuniform FDTD mesh.

The dispersion equation for this formulation of the Yee algorithm can be derived by Fourier-transforming Eqs. (1) and (2) into k,$\omega-$domain. Eliminating the complex $E-$ and $H-$field amplitudes yields

$$\begin{aligned} -2j\, cb_i\, db_i \sin\frac{k_\nu\,\Delta x_i}{2}\,(e^{-j\frac{k_\nu\,\Delta x_i}{2}} - e^{j\frac{k_\nu\,\Delta x_{i-1}}{2}}) \\ = (e^{j\frac{\omega_0\,\Delta t}{2}} - ca_i\, e^{-j\frac{\omega_0\,\Delta t}{2}}) \\ \cdot (e^{j\frac{\omega_0\,\Delta t}{2}} - da_i\, e^{-j\frac{\omega_0\,\Delta t}{2}}) \end{aligned} \tag{7}$$

with k_ν as the numerical wave number at the frequency ω_0.

If ca_i, cb_i, da_i and db_i are replaced by the expressions given in Eqs. (3)–(6) and both the electric and the magnetic losses are neglected, Eq. (7) reduces to

$$\begin{aligned} \frac{1}{(c_0\,\Delta t)^2}\,\sin^2\frac{\omega_0\,\Delta t}{2} \\ = \frac{j}{\Delta x_i\,(\Delta x_i + \Delta x_{i-1})}\,\sin\frac{k_\nu\,\Delta x_i}{2} \\ \cdot (e^{-j\frac{k_\nu\,\Delta x_i}{2}} - e^{j\frac{k_\nu\,\Delta x_{i-1}}{2}}). \end{aligned} \tag{8}$$

For a uniform mesh with $\Delta x_i = \Delta x_{i-1} = \Delta x$, Eq. (8) yields the conventional form of the dispersion equation for the one-dimensional mesh:

$$\frac{1}{\Delta x^2}\sin^2\frac{k_\nu\,\Delta x}{2} = \frac{1}{(c_0\,\Delta t)^2}\sin^2\frac{\omega_0\,\Delta t}{2}. \tag{9}$$

2.2 Properties of the Dispersion Equation

Before discussing the numerical dispersion in nonuniform meshes, two basic characteristics of the uniform dispersion Eq. (9) should be pointed out. At the maximum stable time step $\Delta t_{\max} = \Delta x/c_0$, Eq. (9) reduces to $k_\nu = \pm\omega_0/c_0$ and the algorithm is completely dispersionless. Defining the Courant factor as $CF = \Delta t/\Delta t_{\max}$ with Δt as the actual time step used for the updating and for applying $CF < 1$, the algorithm becomes dispersive. For small time steps, it converges rapidly to the following expression:

$$\frac{c_\nu}{c_0} = \frac{\pi\,\Delta x}{\lambda\,\arcsin\frac{\pi\,\Delta x}{\lambda}} \tag{10}$$

with c_ν as the numerical phase velocity. Figure 2 shows to which extent the dispersion error for a given mesh step size grows as the Courant factor decreases. The error maximum (Eq. (10)) is almost reached at $CF = 0.25$. For high grid resolutions (e.g. better than $\lambda/20$), it remains generally small. In nonuniform meshes, the upper limit of the dispersion error is reached if the largest cells in the grid are four times as large as the smallest cell, which determines the time step. But even in uniform meshes, this effect increases the dispersion error. E. g., a material with an ϵ_r of 16 is also updated with a CF of 0.25 if regions of vacuum are present in the grid.

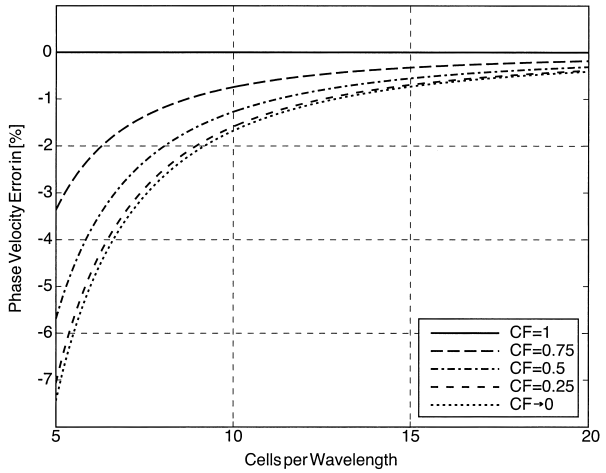

Fig. 2 Numerical phase velocity error for different Courant factors CF as a function of the ratio of wavelength and cell size in a one-dimensional grid.

Table 1 Phase and amplitude errors for a plane wave of 1 GHz ($k_0 = 20.96$/m) in differently graded meshes with a length of 0.3 m, $\Delta x_{\min} = 3$ mm, $\Delta x_{\max} = 30$ mm.

Grad. Steps	Grad. Ratio	30 mm Steps	k_{eff} [1/m]	Phase Error	Ampl. Error
27	1.1:1	none*	21.08+j 0.08	0.57%	2.4%
10	1.3:1	7	21.22+j 0.09	1.27%	2.9%
6	1.5:1	9	21.25+j 0.10	1.40%	3.0%
3	2.5:1	10	21.28+j 0.11	1.52%	3.4%
2	9:1	10	21.28+j 0.14	1.55%	4.3%

*With a grading ratio of 1.1:1, the maximum grid step of 30 mm is not reached within the grid length of 300 mm.

If $\Delta x_i \neq \Delta x_{i-1}$, Eq. (8) can only be solved numerically. In this case, the numerical wave number k_ν will be complex. A wave propagating into the direction of increasing cell size ($\Delta x_i > \Delta x_{i-1}$) will be amplified. Propagating into the opposite direction ($\Delta x_i < \Delta x_{i-1}$), the wave will be attenuated. Since an expression for the complex k_ν cannot be given analytically, the phase errors in nonuniform meshes cannot conveniently be expressed in terms of cell size and grading ratio. Therefore it appears to be more appropriate to present effective numerical wave numbers for specific cases of differently graded meshes. Table 1 shows the effective phase and amplitude errors which a plane wave suffers after traveling through a one-dimensional graded grid calculated with Eq. (8) considering the numerical wave number of each grid cell. The plane wave has a frequency of 1 GHz and the grid size is 0.3 m. The step size in the grid grows as a geometrical series from 3 mm to 30 mm with different grading ratios. As soon as the maximum cell size has been reached, the grid step is kept constant. For the different meshes, the effective numerical wave number is defined as the average of the numerical wave numbers of each cell

$$k_{\text{eff}} = \frac{\sum_{i=0}^{n} k_{\nu_i} \Delta x_i}{\sum_{i=0}^{n} \Delta x_i}, \tag{11}$$

with k_{ν_i} as a function of Δx_i and Δx_{i-1}. The results in Table 1 show that large cells significantly contribute to the eventual phase error. Generally, the amplitude error is in the order of magnitude of three percent. The amplification is restricted to the graded region of the mesh. These findings will be confirmed by numerical experiments in Sect. 3.2.

3. Phase Velocity Correction

The basic idea of the phase velocity correction is to use the wave number and wave impedance instead of the material properties to calculate the update coefficients. Although the wave number is - of course - frequency dependent, it will be demonstrated that the phase velocity correction can yield an overall reduction of the dispersion errors in nonuniform meshes.

3.1 Phase Velocity Corrected Nonuniform FDTD Algorithm

In order to derive the phase velocity corrected form of the nonuniform FDTD algorithm, the E-field update Eq. (1), which has lost its second order accuracy, is rewritten with separate update coefficients for the finite difference terms:

$$E|_i^{n+1} = ca_i\, E|_i^n + cb_{1_i}\, H|_{i+\frac{1}{2}}^{n+\frac{1}{2}} - cb_{2_i}\, H|_{i-\frac{1}{2}}^{n+\frac{1}{2}} \tag{12}$$

For simplicity, the electric losses will be assumed to be zero in the remainder of this section ($ca_i = 1$). Fourier-transforming Eq. (12) into k,$\omega-$domain yields

$$\begin{aligned} &2j\, E_0 \sin\left(\frac{\omega\Delta t}{2}\right) \\ &\quad = H_0 \left(cb_{1_i}\, e^{-j\frac{k_i\Delta x_i}{2}} - cb_{2_i}\, e^{j\frac{k_i\Delta x_{i-1}}{2}}\right) \end{aligned} \tag{13}$$

with k_i as the wave number for the frequency ω_0 in the medium of the cell with the index i. Replacing the E-field amplitude E_0 by $Z_i\, H_0$ leads to[†]

$$2j\, Z_i \sin\frac{\omega\Delta t}{2} = cb_{1_i}\, e^{-j\frac{k_i\Delta x_i}{2}} - cb_{2_i}\, e^{j\frac{k_i\Delta x_{i-1}}{2}}. \tag{14}$$

This complex equation can be solved for the two real update coefficients cb_{1_i} and cb_{2_i}:

$$cb_{1_i} = -\frac{2Z_i \sin\frac{\omega_0\Delta t}{2} \cos\frac{k_i\Delta x_{i-1}}{2}}{X_i} \tag{15}$$

[†]Z_i is the wave impedance of the medium of the cell indexed i. Since the losses are assumed to be zero, k_i and Z_i are real numbers.

$$cb_{2_i} = -\frac{2Z_i \sin\frac{\omega_0\Delta t}{2} \cos\frac{k_0\Delta x_i}{2}}{X_i} \tag{16}$$

with

$$X_i = \sin\frac{k_i\Delta x_i}{2}\cos\frac{k_i\Delta x_{i-1}}{2} + \sin\frac{k_i\Delta x_{i-1}}{2}\cos\frac{k_i\Delta x_i}{2}$$

Here, ω_0 is the optimization frequency of the phase velocity correction at which the algorithm works completely distortionless, and Z_i is the wave impedance of the medium at the corresponding location of the field component in the grid.

Since the H-field update Eq. (2) keeps its central difference in the nonuniform mesh, it is not necessary to use separate update coefficients. The H-field update coefficient db_i can be calculated in the same manner as above, yielding

$$db_i = -\frac{\sin\frac{\omega_0\Delta t}{2}}{Z_i \sin\frac{k_i\Delta x_i}{2}}. \tag{17}$$

If the mesh spacing is uniform ($\Delta x_i = \Delta x_{i-1}$) and a Courant factor of one is used, Eqs. (15)–(17) converge to the expressions for the conventional FDTD algorithm Eqs. (4) and (6). Since the maximum stable time step in nonuniform meshes is determined by the smallest mesh cell, the same stability criterium as for the original Yee-algorithm can be applied.

For lossy material, the coefficients ca_i and da_i must be considered in the Fourier transforms of the update equations, leading to expressions for the update coefficients different from Eqs. (15)–(17). In order to derive the update coefficients for lossy media, ca_i and da_i can be used as given in Eqs. (3) and (5). It is important to note that separate coefficients db_{1_i} and db_{2_i} have to be introduced for the H-field update equation, if lossy media are used.

3.2 Dispersion Properties of the Corrected Algorithm

The numerical dispersion of the corrected algorithm can be calculated as described in Sect. 2.1. According to Eq. (10), an expression for the phase velocity error for small time steps ($CF \to 0$) can be derived. In order to obtain a real value for the numerical phase velocity, uniform mesh spacing ($\Delta x_i = \Delta x_{i-1}$) is assumed. The phase velocity error can then be written as

$$\frac{c_\nu}{c_0} = \frac{\omega_0\,\Delta x}{2\,c_0 \arcsin(\frac{\omega}{\omega_0}\sin\frac{\omega_0\,\Delta x}{2\,c_0})}. \tag{18}$$

Figure 3 shows the dispersion properties of the phase velocity corrected algorithm in comparison to those of the conventional one. For all mesh step sizes, the corrected algorithm yields the accurate phase velocity at the optimization frequency ω_0. Although the algorithm remains dispersive, it shows a reduced phase velocity error for all frequencies above ω_0. At lower frequencies, the phase velocity error of the conventional FDTD scheme approaches zero, whereas it increases for the corrected algorithm. However, from Eqs. (10) and (18) ω_0 can be calculated such that an overall dispersion reduction is achieved in the frequency range of interest.

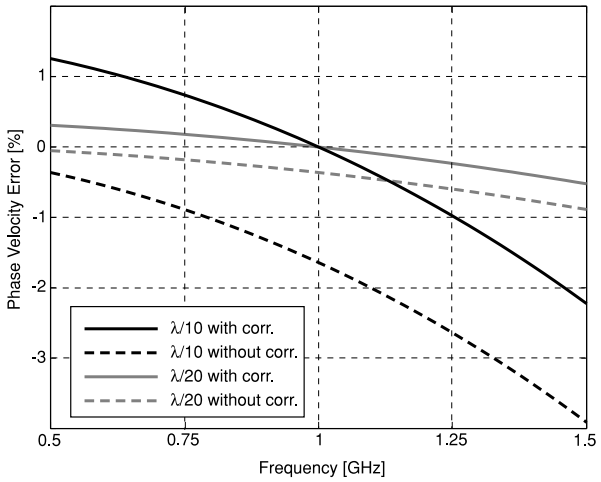

Fig. 3 Numerical phase velocity error for $CF \to 0$ with and without correction for 1 GHz and different cell sizes in a one-dimensional grid.

From Fig. 3 also follows, that there is a certain bandwidth within which the phase errors of the corrected algorithm remain below a given maximum. This bandwidth depends on the ratio of cell size and wavelength. If e.g. the resonance frequency of a structure is only roughly known (from theory or from a non-corrected FDTD simulation), its accurate value can be determined by a simulation with the corrected algorithm. An approximate value for the resonance frequency can be used as optimization frequency ω_0 and the maximum cell size can be limited such that the expected deviations are covered by the bandwidth within which the errors of the corrected algorithm are close to zero.

Figure 4 shows the wave front of a plane wave with a linearly rising envelope after propagating 12 m through a nonuniform mesh. The wave simulated with the corrected algorithm travels with the right phase velocity, whereas the numerical phase velocity of the conventional FDTD scheme is too low. The wave front calculated with the corrected algorithm is distorted as well because of transients in the signal.

Figure 5 demonstrates the amplitude distortion due to the mesh grading[†]. Whereas the amplitudes of the waves in the simulations without correction rise or fall as predicted in Sect. 2.2, the wave keeps its am-

[†]In order to avoid spurious reflections from the grid boundaries, the size of the one dimensional grid has been chosen such that the reflected waves did not reach the range depicted in Fig. 5.

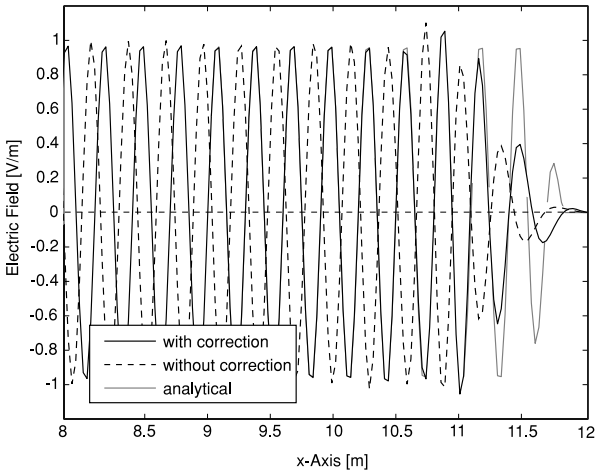

Fig. 4 Front of a plane wave (1 GHz) with linear envelope in a graded mesh ($\Delta x_{\max} = \lambda/10$, $\Delta x_i/\Delta x_{i-1}$=1.0025) after propagating a distance of 12 m from the source.

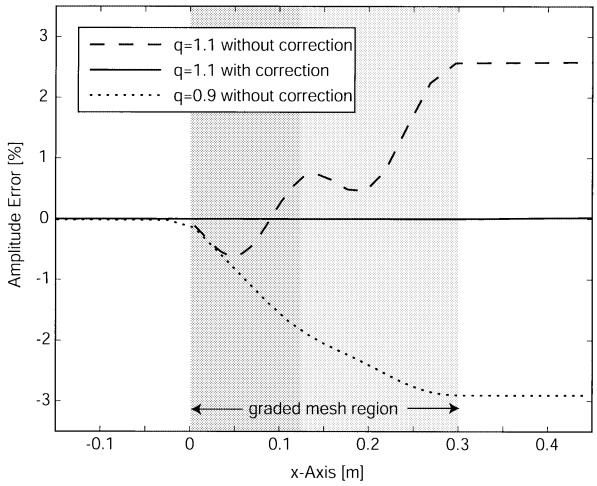

Fig. 5 Amplitude of a plane wave of 1 GHz in different graded meshes with and without dispersion correction. $q = \Delta x_i/\Delta x_{i-1}$, $\Delta x_{\min} = 3\,\text{mm}$ and $\Delta x_{\max} = 30\,\text{mm}$.

plitude if the phase velocity correction is applied. The complete compensation of the spurious amplification or attenuation is of course only possible at the optimization frequency ω_0.

4. Extension to Three Dimensions

The dispersion characteristics of the one-dimensional finite-difference algorithm as described in Sect. 2 are also true for its three-dimensional formulation. Additionally, the numerical phase velocity error is dependent on the propagation direction.

In three dimensions, the phase velocity correction also allows error correction for a particular frequency. However, the anisotropic dispersion characteristics of the FDTD-algorithm remain, though it is possible to compensate the phase velocity errors for an arbitrary angle of propagation.

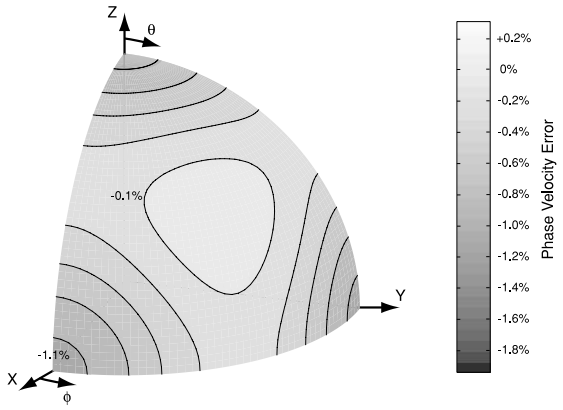

Fig. 6 Numerical phase velocity error as a function of φ and ϑ for a cell size of $\lambda/10$ and $CF \to 0$. Average error $\varsigma = 0.54\%$.

4.1 Numerical Dispersion of the Three-Dimensional Algorithm

The generalized form of the dispersion equation of the three-dimensional FDTD scheme (A·1) is given in Appendix. Inserting the conventional update coefficients [2] into Eq. (A·1) yields the three-dimensional dispersion equation for the uniform grid:

$$\frac{1}{(c_0\,\Delta t)^2}\,\sin^2\frac{\omega_0\,\Delta t}{2} = \frac{1}{\Delta x^2}\,\sin^2\frac{u_x\,k_\nu\,\Delta x}{2} + \frac{1}{\Delta y^2}\,\sin^2\frac{u_y\,k_\nu\,\Delta y}{2} + \frac{1}{\Delta z^2}\,\sin^2\frac{u_z\,k_\nu\,\Delta z}{2} \qquad (19)$$

with the numerical wave vector

$$\mathbf{k}_\nu = k_\nu \cdot \begin{pmatrix} u_x \\ u_y \\ u_z \end{pmatrix}$$

and u_x, u_y and u_z as the coefficients of the unit vector of the direction of $\mathbf{k}_\nu$.

Figure 6 shows the numerical phase velocity error as a function of φ and ϑ in a uniform mesh for $\Delta x = \Delta y = \Delta z = \lambda/10$ and $CF = 1$. A wave in the mesh propagates along the cell diagonal without phase distortion, whereas the maximum phase velocity error occurs for propagation along the axes. From Eq. (19) it is clear that the FDTD algorithm is dispersive for all directions but the cell diagonal. For $CF \to 0$, the dispersion properties of the algorithm increase up to 1.7% (Fig. 7). These figures may appear small, but a phase velocity error of only 1.7% will lead to a complete phase inversion after only 30 wavelengths (See also Fig. 4). In order to allow better comparison of the 3D-dispersion properties, the following definition of the average phase velocity error of a mesh cell with the indices i, j and k will be used:

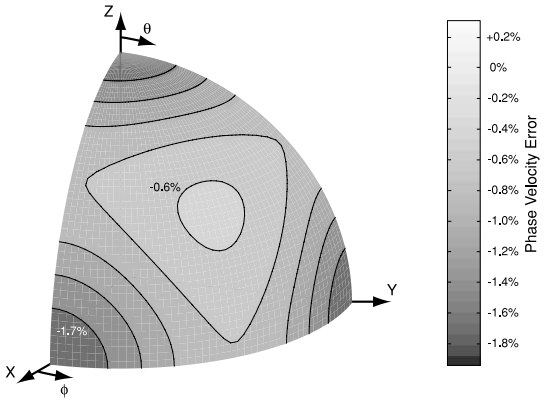

Fig. 7 Numerical phase velocity error as a function of φ and ϑ for a cell size of $\lambda/10$ and $CF \to 0$. Average error $\varsigma = 1.06\%$.

$$\varsigma_{i,j,k} = \sqrt{\frac{2}{\pi}\int_0^{\frac{\pi}{2}}\int_0^{\frac{\pi}{2}}\left(\frac{c_{\nu_{i,j,k}}(\varphi,\vartheta)}{c_0}-1\right)^2 \sin\vartheta\, d\varphi\, d\vartheta} \quad (20)$$

For a Courant factor of 1 and a cell size of $\lambda/10$, the average phase velocity error ς is 0.54%, and if the Courant factor approaches zero, ς increases to 1.06%.

4.2 Corrected Update Coefficients

The corrected update coefficients for the three-dimensional algorithm are derived in a similar way as for the one-dimensional form. A detailed demonstration will be given for the E_y-update equation with separate coefficients

$$\begin{aligned} E_y|^{n+1}_{i,j+\frac{1}{2},k} &= ca_{i,j,k}\, E_y|^{n}_{i,j+\frac{1}{2},k} \\ &\quad + cbz_{1_{i,j,k}}\, H_x|^{n+\frac{1}{2}}_{i,j+\frac{1}{2},k+\frac{1}{2}} \\ &\quad - cbz_{2_{i,j,k}}\, H_x|^{n+\frac{1}{2}}_{i,j+\frac{1}{2},k-\frac{1}{2}} \\ &\quad - cbx_{1_{i,j,k}}\, H_z|^{n+\frac{1}{2}}_{i+\frac{1}{2},j+\frac{1}{2},k} \\ &\quad + cbx_{2_{i,j,k}}\, H_z|^{n+\frac{1}{2}}_{i-\frac{1}{2},j+\frac{1}{2},k}. \end{aligned} \quad (21)$$

The E-field components in this equation are substituted by

$$E_y|^{n}_{i,j,k} = Z_m\,(u_x\, H_z|^{n}_{i,j,k} - u_z\, H_x|^{n}_{i,j,k}) \quad (22)$$

with Z_m as the wave impedance of the medium at the corresponding location of the mesh $m_{i,j,k}$. u_x and u_z are the x- and z-components of the unit vector of the propagation direction for which the phase velocity errors are to be compensated. Fourier-transforming the resulting expression into k,ω-domain then yields

$$\begin{aligned} &Z_m\,(u_x\, H_z - u_z\, H_x)\,(e^{j\frac{\omega_0\,\Delta t}{2}} - ca_{i,j,k}\, e^{-j\frac{\omega_0\,\Delta t}{2}}) \\ &\quad = H_x\,(cbz_{1_{i,j,k}}\, e^{-j\frac{u_z\, k_m\, \Delta z_k}{2}} \\ &\qquad - cbz_{2_{i,j,k}}\, e^{j\frac{u_z\, k_m\, \Delta z_{k-1}}{2}}) \\ &\qquad - H_z\,(cbx_{1_{i,j,k}}\, e^{-j\frac{u_x\, k_m\, \Delta x_i}{2}} \\ &\qquad - cbx_{2_{i,j,k}}\, e^{j\frac{u_x\, k_m\, \Delta x_{i-1}}{2}}) \end{aligned} \quad (23)$$

with k_m as the wave number at the frequency of optimization ω_0 in the medium indexed $m_{i,j,k}$. Equation (23) can be split up into two separate expressions containing either the H_x- or the H_z-components, which can then be eliminated. The equation for the H_z-components reads

$$\begin{aligned} &u_x\, Z_m\,(e^{j\frac{\omega_0\,\Delta t}{2}} - ca_{i,j,k}\, e^{-j\frac{\omega_0\,\Delta t}{2}}) \\ &\quad = cbx_{2_{i,j,k}}\, e^{j\frac{u_x\, k_m\, \Delta x_{i-1}}{2}} \\ &\qquad - cbx_{1_{i,j,k}}\, e^{-j\frac{u_x\, k_m\, \Delta x_i}{2}}. \end{aligned} \quad (24)$$

As already mentioned in Sect. 3.1, $ca_{i,j,k}$ can be used as in the conventional FDTD formulation. The resulting complex equation can then be solved for the two remaining real update coefficients $cbx_{1_{i,j,k}}$ and $cbx_{2_{i,j,k}}$. Solving for $cbx_{1_{i,j,k}}$ in a lossless medium ($ca_{i,j,k} = 1$) yields

$$cbx_{1_{i,j,k}} = \frac{2\, u_x Z_m\, \sin\frac{\omega_0\Delta t}{2}\, \cos\frac{u_x k_m \Delta x_{i-1,j,k}}{2}}{X_{i,j,k}} \quad (25)$$

with

$$\begin{aligned} X_{i,j,k} &= \sin\frac{u_x k_m \Delta x_{i,j,k}}{2}\, \cos\frac{u_x k_m \Delta x_{i-1,j,k}}{2} \\ &\quad + \sin\frac{u_x k_m \Delta x_{i-1,j,k}}{2}\, \cos\frac{u_x k_m \Delta x_{i,j,k}}{2}. \end{aligned}$$

The coefficients of the remaining update equations are derived analogously.

For propagation directions along one of the mesh axes, the unit vector coefficients u_x, u_y or u_z can be zero. Calculating the limit of Eq. (25) for $u_{x,y,z} \to 0$ then yields

$$cbx_{1_{i,j,k}} = \frac{4\, Z_m \sin\frac{\omega_0\Delta t}{2}}{k_m(\Delta x_{i,j,k} + \Delta x_{i-1,j,k})}. \quad (26)$$

4.3 Dispersion Properties of the Corrected Algorithm

The numerical phase velocity of the corrected algorithm retains its anisotropic characteristics. However, as in the one-dimensional scheme a complete compensation of the grading effects can be achieved for one frequency ω_0. In this case the distribution of the phase velocity error is the same as for a homogeneous mesh with $CF = 1$ (See Fig. 6), and the accuracy of the second-order scheme is therefore recovered.

A comparison between the averaged error ς of the corrected and the conventional three-dimensional FDTD algorithms for $\Delta t \to 0$ is shown in Fig. 8. The coefficients are optimized for a frequency of 1 GHz and propagation angles along the diagonal of a cube. The

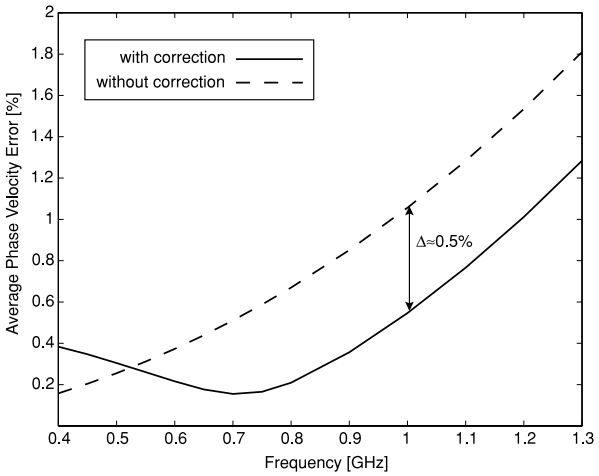

Fig. 8 Averaged phase velocity error ς for a cell size of $\lambda/10$ at 1 GHz with and without phase velocity correction for 1 GHz.

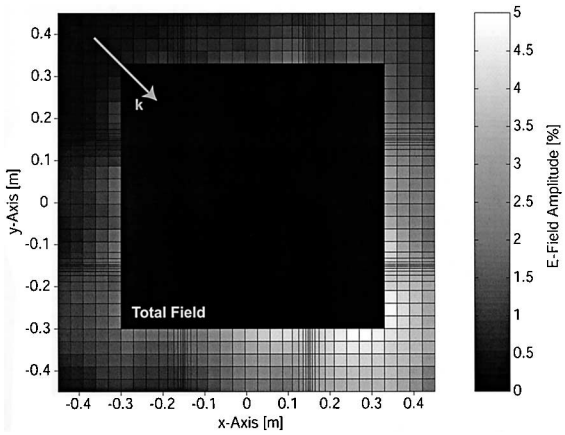

Fig. 9 Spurious E-field in the scattered field region caused by numerical dispersion at an incidence angle of $\varphi_0 = 45°$ and $\vartheta_0 = 54.7°$ *without* phase velocity correction. The maximum cell size is $\lambda/10$.

side lengths of the cell are $\lambda/10$. The error ς of the corrected algorithm has a minimum at approximately 700 MHz, whereas the error of the conventional scheme steadily approaches zero for lower frequencies. For all frequencies above 700 MHz, the difference between the errors of the corrected algorithm and the conventional one is an almost constant value of approximately 0.5%. This means that an error reduction of about 50% can be achieved at the optimization frequency.

4.4 Plane Wave Excitation

In the finite calculation domain of a Yee grid, plane wave excitation is realized using the Total-Field-Scattered-Field (TFSF) formulation [21]. Here, only a limited area of the mesh, the total-field region, is illuminated with a plane wave. The analytical solution of the plane wave is then subtracted at the boundaries of this region such that the outer part of the grid only contains the scattered field. This requires the precise knowledge of the amplitude and the phase of the exciting plane wave. For uniform meshes, the exciting wave can be calculated using the numerical phase velocity for the particular direction of propagation. For nonuniform meshes, this is an infeasible task, because the phase distortion has to be considered for all the cells the exciting wave traverses. If the mesh is electrically large, subtracting the analytical solution of a plane wave will generate spurious field components at the boundaries of the total-field region because of the phase distortion which the wave has suffered propagating through the nonuniform mesh. The application of the phase velocity corrected algorithm allows a plane wave to propagate through an arbitrarily spaced mesh without any phase distortion and therefore enables the usage of the TFSF formulation for electrically large nonuniform meshes.

Figure 9 shows the E-field outside the total field region of an *empty* nonuniform mesh with a maximum

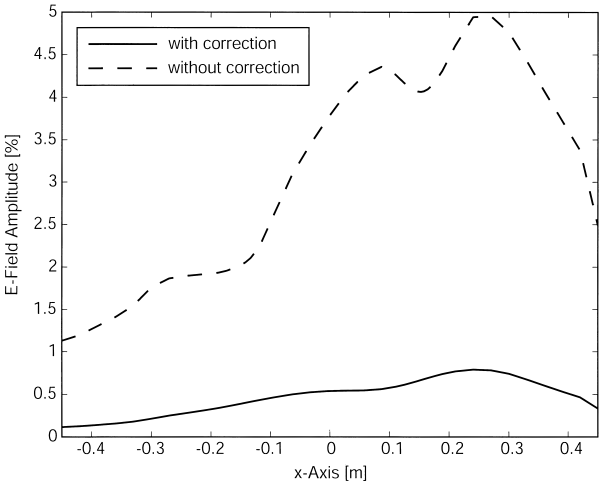

Fig. 10 Amplitude of the spurious E-field along the x-axis at the boundary of the total field region ($y = -0.3$ m, see Fig. 9).

cell size of $\lambda/10$. The side length of the total field region is approximately two wavelengths. The wave has traveled along the diagonal of the cubical total field region ($\sqrt{3}\,\lambda$) with a phase velocity error of approximately 0.6% (Fig. 7). Since there is no scatterer in the mesh, the fields occurring outside this region are due to the above mentioned phase differences between the analytical field and the distorted wave which has traveled through the nonuniform grid. In this example, spurious E-fields with an amplitude of up to 5.0% of the total field occur (Fig. 9). In Fig. 10, the improvement achieved by the corrected algorithm is shown. The maximum E-field components outside the total field region have an amplitude of less than 0.8% of the excited plane wave. The remaining error is due to the envelope of the exciting signal. It contains components of very high frequencies which do not propagate properly through the mesh.

5. Examples

The improvements which can be achieved with the phase velocity corrected algorithm will be shown with the help of two examples: First, the field distribution in a dielectric sphere illuminated by a plane wave will be calculated. As an application, the influence of the mesh grading on the feedpoint impedance of a patch antenna will be demonstrated.

5.1 Dielectric Sphere

Since FDTD has often been used to calculate the absorption of electromagnetic energy in biological objects [22], [23], the plane wave excitation using the TFSF formulation is demonstrated with the help of a sphere with the dielectric parameters of brain tissue (ϵ_r=42, σ=0.85 S/m) [24]. The sphere has a radius of 0.1 m (approximately the dimensions of a human head) and is illuminated with a plane wave of 900 MHz. The direction of the Poynting vector of the incident wave is set to $\varphi_0 = 45°$ and $\vartheta_0 = 54.7°$. A reference calculation is performed with the Generalized Multipole Technique (GMT) [25]. For an application of this kind, the numerical uncertainties of GMT can be neglected with respect to the analytical solution [26]. Figure 11 shows the dielectric sphere and the polarization of the incoming wave, together with the field distribution calculated with GMT.

The FDTD model of the discretized sphere is shown in Fig. 12. The dimensions of the computational domain are $0.6 \times 0.6 \times 0.6\,\mathrm{m}^3$. The maximum grid step in free space is 20 mm. In the sphere it is limited to 5 mm because of the shorter wavelength in the dielectric. The minimum grid spacing is 1 mm. The total field area is placed closely around the sphere in order to keep it small in terms of wavelengths to reduce the errors due to the phase distortions. The propagation direction of the plane wave of $\varphi_0 = 45°$ and $\vartheta_0 = 54.7°$ was chosen to keep the phase errors of the non-corrected calculation as small as possible. The mesh consists of approximately 650 000 cells. PML absorbing boundary conditions [27] are used to truncate the mesh.

Since the FDTD algorithm uses a rectilinear grid, high errors occur due to staircasing effects if round objects are modeled. These errors are not the subject of this paper and will therefore not be dealt with any further. Figures 13 and 14 show the error of the E-field amplitude inside the sphere for a calculation with the conventional FDTD algorithm and with phase velocity correction. The maximum error in the non-corrected simulation compared to the reference solution at the same location is approximately 25%. By application of the phase velocity corrected algorithm, the overall error of the field distribution in the sphere can be significantly reduced. Figure 14 shows maximum errors of less than 9%.

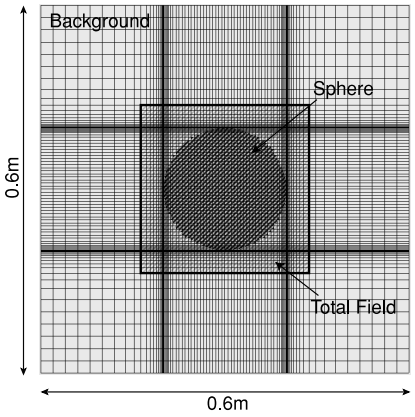

Fig. 12 Dielectric sphere with TFSF excitation in a nonuniform mesh of the size $0.6 \times 0.6 \times 0.6\,\mathrm{m}^3$.

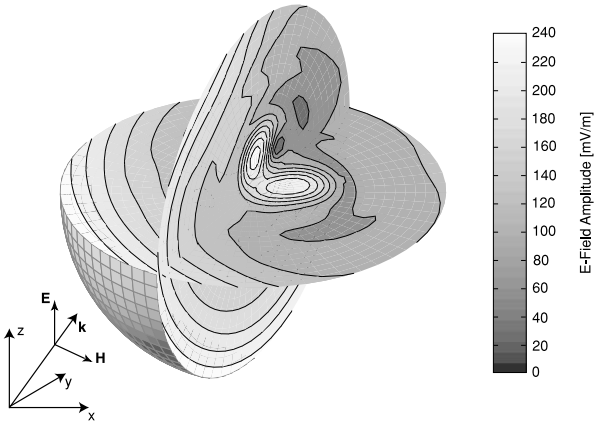

Fig. 11 Distribution of the electric field in a dielectric sphere (ϵ_r=42, σ=0.85 S/m) excited by a plane wave of 900 MHz and 1 V/m.

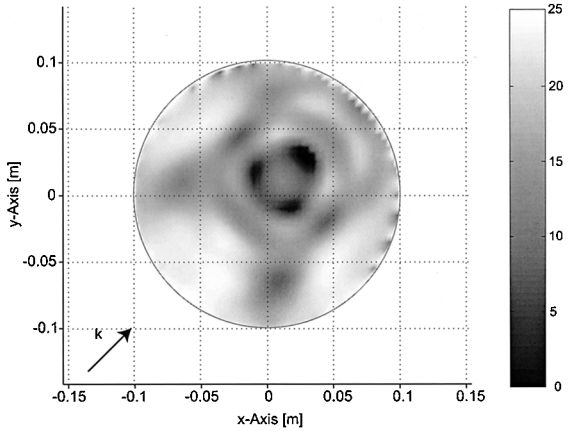

Fig. 13 Absolute value of the E-field error in the z-normal plane of the dielectric sphere calculated *without* phase velocity correction.

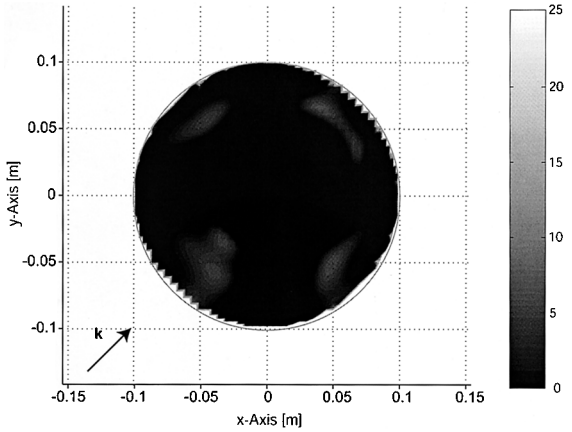

Fig. 14 Absolute value of the E-field error in the z-normal plane of the dielectric sphere calculated *with* phase velocity correction.

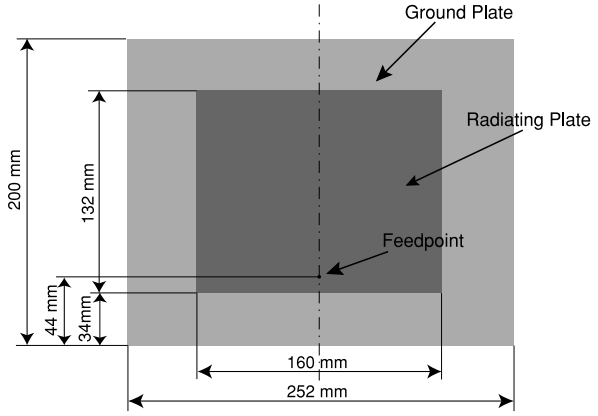

Fig. 15 Patch antenna for 1 GHz. The plate distance is 6 mm.

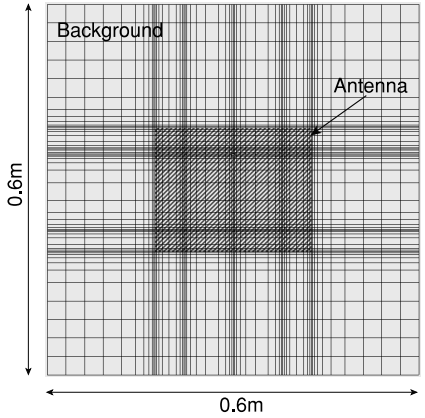

Fig. 16 Patch antenna in a nonuniform mesh with a size of $0.6 \times 0.6 \times 0.6\,\mathrm{m}^3$ and a maximum grading ratio of 1.8.

5.2 Patch Antenna

In order to obtain reliable results for antenna simulations with FDTD, the calculation domain must be chosen such that the reactive field of the antenna is not cut off by the absorbing boundary conditions. This generally leads to a large number of mesh cells even if nonuniform mesh steps are used. Because of the reduced phase velocity in larger cells, the calculated resonance frequencies of the antenna will be too low [28]. This error can be reduced by the application of the phase velocity corrected algorithm.

The described effect is demonstrated with the help of a simple patch antenna structure for a frequency of 1 GHz. It consists of two perfectly conducting plates suspended in air. The exact dimensions of the antenna are given in Fig. 15. The feedpoint impedance of the antenna is calculated using a nonuniform mesh with a maximum grading ratio $\Delta x_i/\Delta x_{i-1}$ of 1.8 (See Fig. 16). On all material boundaries, the step size in the mesh is reduced to a minimum of 2 mm. The maximum step size is limited to 30 mm, which corresponds to $\lambda/10$ at 1 GHz. The antenna is placed into a computational domain of $0.6 \times 0.6 \times 0.6\,\mathrm{m}^3$ which leads to a number of approximately 90 000 mesh cells. A reference calculation is carried out with a high resolution uniform mesh. In order to avoid influences of different discretizations of the material discontinuities, the uniform mesh uses an overall cell size of $2 \times 2 \times 2\,\mathrm{mm}^3$. Otherwise, the edges and corners of the metal patches of the antenna would require additional corrections [29]–[31]. The uniform mesh has the same dimensions as the graded mesh and therefore consists of 27 million cells. Again, the meshes are truncated with PML absorbing boundary conditions.

Because of the high resolution of the uniform mesh, the numerical phase velocity errors are negligible. For the largest cells in the nonuniform mesh, the smallest average dispersion error ς of 0.3 is reached at an optimization frequency of 1.3 GHz (See also Fig. 8). The minimum of ς can be found numerically from Eq. (A· 1).

The calculated real and imaginary parts of the feedpoint impedance for the different meshes and optimization frequencies are displayed in Figs. 17 and 18. The conventional nonuniform FDTD algorithm calculates a resonance frequency approximately 2.5% below the reference result in the high resolution uniform mesh. The phase velocity corrected algorithm reduces this error by approximately 50%.

6. Conclusion

A novel method has been proposed to correct the numerical phase velocity errors in nonuniform FDTD meshes. The method is based on a reformulation of the FDTD update equations with separate coefficients for the finite-difference terms. The numerical properties of the method have been analyzed both theoretically and with simulation examples.

The analysis of the dispersion properties of the nonuniform FDTD algorithm has shown that the grading of the mesh leads to a complex numerical wave num-

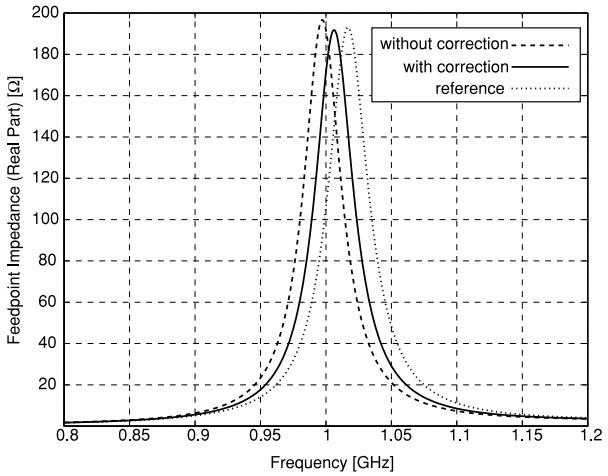

Fig. 17 Real part of the feedpoint impedance for optimization frequencies f_0 of 1 GHz and 1.35 GHz and without phase velocity correction in comparison to the reference calculation.

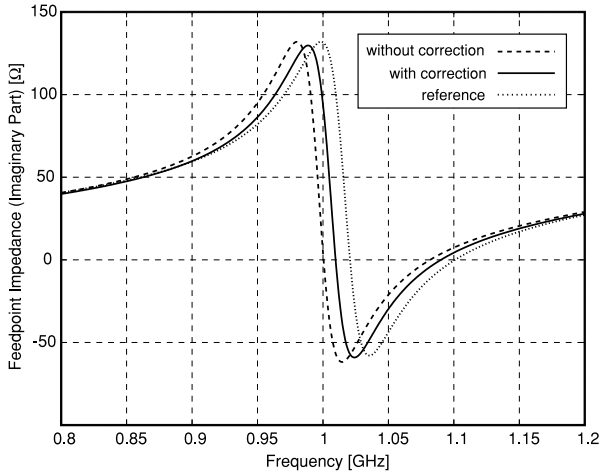

Fig. 18 Imaginary part of the feedpoint impedance for optimization frequencies f_0 of 1 GHz and 1.35 GHz and without phase velocity correction in comparison to the reference calculation.

ber, which is the reason for spurious amplification or attenuation and increased phase errors.

The method proposed in this paper yields a general reduction of the numerical dispersion in nonuniform meshes and completely compensates phase and amplitude errors for a particular frequency of optimization. For this frequency, the accuracy of the original second order scheme is recovered. Additionally, a direction can be chosen into which a plane wave can propagate completely distortionless. This also enables the use of the TFSF formulation together with electrically large nonuniform meshes.

Two benchmark examples, a patch antenna simulation and a dielectric sphere under incidence of a plane wave, have been conducted. They have shown that the novel phase velocity corrected algorithm yields the same flexibility and robustness as the original FDTD scheme and significantly increases the accuracy of the simulation results in nonuniform meshes.

Acknowledgements

The authors would like to thank Theodore Samaras for numerous fruitful discussions and Pascal Leuchtmann for his advice about the GMT calculations. The project was supported by the Swiss priority program MINAST and by Schmid & Partner Engineering AG.

References

[1] K.S. Yee, "Numerical solution of initial boundary value problems involving Maxwell's equations in isotropic media," IEEE Trans. Antennas & Propag., vol.14, no.3, pp.585–589, 1966.

[2] A. Taflove and S.C. Hagness, Computational Electromagnetics: The Finite-Difference Time-Domain Method, Second ed., Artech House, Boston and London, 2000.

[3] K.S. Kunz and R.J. Luebbers, Finite Difference Time Domain Mehtod for Electromagnetics, CRC Press, Boca Raton, FL, 1993.

[4] D.M. Sullivan, Electromagnetic Simulation Using the FDTD Method, IEEE Press, New York, 2000.

[5] M.A. Jensen and Y. Rahmat-Samii, "EM interaction of handset antennas and a human in personal communications," Proc. IEEE, vol.83, no.1, pp.7–17, 1995.

[6] S. Chebolu and R. Mittra, "The analysis of microwave antennas using the FDTD method," Microwave Journal, vol.39, no.1, pp.134–150, 1996.

[7] M. Okoniewski and M.A. Stuchly, "A study of the handset antenna and human body interaction," IEEE Trans. Microwave Theory & Tech., vol.44, no.10, pp.1855–1864, Oct. 1996.

[8] P. Monk and E. Süli, "Error estimates for Yee's method on non-uniform grids," IEEE Trans. Magn., vol.30, no.5, pp.3200–3203, Sept. 1994.

[9] D.H. Choi and W.J.R. Hoefer, "A graded mesh FD-TD algorithm for eigenvalue problems," 17th European Microwave Conference Digest, pp.413–417, 1987.

[10] V.J. Branković, D.V. Krupežević, and F. Arndt, "An efficient two-dimensional graded mesh finite-difference time-domain algorithm for shielded or open waveguide structures," IEEE Trans. Microwave Theory & Tech., vol.40, no.12, pp.2272–2277, Dec. 1992.

[11] E.A. Navarro, N.T. Sangary, and J. Litva, "Some considerations on the accuracy of the nonuniform FDTD method and its application to waveguide analysis when combined with the perfectly matched layer technique," IEEE Trans. Microwave Theory & Tech., vol.44, no.7, pp.1115–1124, July 1996.

[12] B.-Q. Gao and O.P. Gandhi, "An expanding-grid algorithm for the finite-difference time-domain method," IEEE Trans. Electromag. Compat., vol.34, no.3, pp.277–283, Aug. 1992.

[13] W. Heinrich, K. Beilenhoff, P. Mezzanotte, and L. Roselli, "Optimum mesh grading for finite-difference method," IEEE Trans. Microwave Theory & Tech., vol.44, no.9, pp.1569–1574, Sept. 1996.

[14] S. Xiao and R. Vahldieck, "A fast analysis of guided wave structures using a continuously variable mesh with second order accuracy," J. IETE, vol.41, no.1, pp.3–14, Jan.–Feb. 1995.

[15] R.C. Tupynambá and A.S. Omar, "Comparison between FDTD graded grids," IEEE MTT-Symposium Digest,

pp.905–908, 1998.
[16] J.B. Schneider and C.L. Wagner, "FDTD dispersion revisited: Faster-than-light propagation," IEEE Microwave & Guided Wave Letters, vol.9, no.2, pp.54–56, Feb. 1999.
[17] J.W. Nehrbass, J.O. Jetvić, and R. Lee, "Reducing the phase error for finite difference methods without increasing the order," IEEE Trans. Antennas & Propag., vol.46, no.8, pp.1194–1201, Aug. 1998.
[18] J.S. Juntunen and T.D. Tsiboukis, "Reduction of numerical dispersion in FDTD method through artificial anisotropy," IEEE Trans. Microwave Theory & Tech., vol.48, no.4, pp.582–588, April 2000.
[19] K. Suzuki, T. Kashiwa, and Y. Hosoya, "Reducing the numerical dispersion in the FDTD analysis by modifying anisotropically the speed of light," Electronics and Communications in Japan, Part 2, vol.85, no.1, pp.50–58, 2002.
[20] J. Svigelj and R. Mittra, "Grid dispersion error using the nonuniform finite-difference-time-domain method," Microwave and Optical Technology Letters, vol.10, no.4, pp.199–201, Nov. 1995.
[21] K.R. Umashankar and A. Taflove, "A novel method to analyze electromagnetic scattering of complex objects," IEEE Trans. Electromag. Compat., vol.24, pp.397–405, 1982.
[22] V. Hombach, K. Meier, M. Burkhardt, E. Kühn, and N. Kuster, "The dependence of EM energy absorption upon human head modeling at 900 MHz," IEEE Trans. Microwave Theory & Tech., vol. 44, no.10, pp.1865–1873, Oct. 1996.
[23] F. Schönborn, M. Burkhardt, and N. Kuster, "The difference of EM energy absorption between adults and children," Health Physics, vol.74, no.2, pp.160–168, Feb. 1998.
[24] C. Gabriel, S. Gabriel, and E. Corthout, "The dielectric properties of biological tissues: I. literature survey," Phys. Med. Biol., vol.41, pp.2231–2249, 1996.
[25] C. Hafner, The Generalized Multipole Technique for Computational Electromagnetics, Artech House, Norwood, MA 1990.
[26] N. Kuster, "Multiple multipole method for simulating EM problems involving biological bodies," IEEE Trans. Biomed. Eng., vol.40, no.7, pp.611–620, July 1993.
[27] J.-P. Berenger, "Three-dimensional perfectly matched layer for the absorption of electromagnetic waves," J. Computational Physics, vol.127, pp.363–379, 1996.
[28] A. Christ, K. Poković, M. Burkhardt, and N. Kuster, "Sensitivity analysis of a planar antenna with respect to FDTD modeling," in USNC/URSI National Radio Science Meeting, p.274, Atlanta, GA, USA, June 1998.
[29] D.B. Shorthouse and C.J. Railton, "The incorporation of static field solutions into the finite difference time domain algorithm," IEEE Trans. Microwave Theory & Tech., vol.40, no.5, pp.986–994, May 1992.
[30] K.R. Umashankar, A. Taflove, and B. Beker, "Calculation and experimental validation of induced currents on coupled wires in an arbitrary shaped cavity," IEEE Trans. Antennas & Propag., vol.35, no.11, pp.1248–1257, 1987.
[31] L. Cascio, G. Tardioli, T. Rozzi, and W.J.R. Hoefer, "A quasi-static modification of TLM at knife edge and 90° wedge singularities," IEEE Trans. Microwave Theory & Tech., vol.44, no.12, pp.2519–2524, Dec. 1996.

Appendix: Dispersion Equation of the Corrected Algorithm

The generalized form of the three-dimensional FDTD dispersion equation can be derived by Fourier-transforming the update equations with separate coefficients (See Eq. (21)) into the k,ω-domain. The determinant of the resulting system of equations for the E- and H-fields has then to be set to zero and solved for the numerical wave number $\mathbf{k}_\nu$.

$$\begin{vmatrix} 0 & a_{12} & a_{13} & a_{14} & 0 & 0 \\ a_{21} & 0 & a_{23} & 0 & a_{25} & 0 \\ a_{31} & a_{32} & 0 & 0 & 0 & a_{36} \\ a_{41} & 0 & 0 & 0 & a_{45} & a_{46} \\ 0 & a_{52} & 0 & a_{54} & 0 & a_{56} \\ 0 & 0 & a_{63} & a_{64} & a_{65} & 0 \end{vmatrix} = 0 \qquad (\mathrm{A}\cdot 1)$$

with

$$\begin{aligned}
a_{12} &= -a_{21} = cbz_{2_{i,j,k}}\, e^{-j\frac{u_z\, k_\nu\, \Delta z_k}{2}} \\
&\quad - cbz_{1_{i,j,k}}\, e^{j\frac{u_z\, k_\nu\, \Delta z_k}{2}} \\
a_{31} &= -a_{13} = cby_{2_{i,j,k}}\, e^{-j\frac{u_y\, k_\nu\, \Delta y_j}{2}} \\
&\quad - cby_{1_{i,j,k}}\, e^{j\frac{u_y\, k_\nu\, \Delta y_j}{2}} \\
a_{23} &= -a_{32} = cbx_{2_{i,j,k}}\, e^{-j\frac{u_x\, k_\nu\, \Delta x_i}{2}} \\
&\quad - cbx_{1_{i,j,k}}\, e^{j\frac{u_x\, k_\nu\, \Delta x_i}{2}} \\
a_{54} &= -a_{45} = dbz_{2_{i,j,k}}\, e^{-j\frac{u_z\, k_\nu\, \Delta z_{k-1}}{2}} \\
&\quad - dbz_{1_{i,j,k}}\, e^{j\frac{u_z\, k_\nu\, \Delta z_k}{2}} \\
a_{46} &= -a_{64} = dby_{2_{i,j,k}}\, e^{-j\frac{u_y\, k_\nu\, \Delta y_{j-1}}{2}} \\
&\quad - dby_{1_{i,j,k}}\, e^{j\frac{u_y\, k_\nu\, \Delta y_j}{2}} \\
a_{65} &= -a_{56} = dbx_{2_{i,j,k}}\, e^{-j\frac{u_x\, k_\nu\, \Delta x_{i-1}}{2}} \\
&\quad - dbx_{1_{i,j,k}}\, e^{j\frac{u_x\, k_\nu\, \Delta x_i}{2}} \\
a_{14} &= a_{25} = a_{36} = e^{j\frac{\omega_0\, \Delta t}{2}} - ca_{i,j,k}\, e^{-j\frac{\omega_0\, \Delta t}{2}} \\
a_{41} &= a_{52} = a_{63} = e^{j\frac{\omega_0\, \Delta t}{2}} - da_{i,j,k}\, e^{-j\frac{\omega_0\, \Delta t}{2}}.
\end{aligned}$$

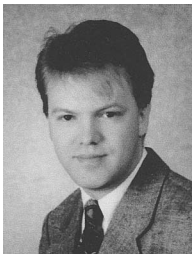

Andreas Christ was born 1968 in Offenbach, Germany. 1996 he received his M.S. degree in Electrical Engineering from the Technical University Darmstadt. In 1997, he joined the Bioelectromagnetics/EMC Group at the Swiss Federal Institute of Technology (ETH) in Zürich, Switzerland. There, he was involved in the numerical simulation of antennas, dosimetric probes and human head models for dosimetric studies as well as the development of an integrated FDTD simulation platform optimized for this range of applications. Since 1999 he has continued his work at the Integrated Systems Laboratory at ETH where he was also involved in the simulation of optical devices. Currently, he is finishing his PhD thesis.

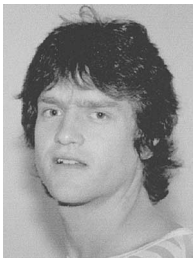

Jürg Fröhlich was born in Thun, Switzerland in November 1964. He received the M.S. and Ph.D. degrees in Electrical Engineering from the Swiss Federal Institute of Technology (ETH) in Zürich. 1990 he joined the Laboratory of Electromagnetic Fields and Microwave Electronics at ETH. There he worked on the modeling of EMC problems using the Generalized Multipole Technique (GMT) and developed optimization algorithms based on evolutionary computation for device design problems. 1997, he joined the Bioelectromagnetics/EMC Group (BIOEM/EMC) where he was involved in the development of a Simulation Platform for Antenna Design and Dosimetry and the conduction of compliance tests using the DASY 3 Near Field Scanner. From 1999 to March 2000 he worked at the Institute of Operations Research of the University in Zürich where he developed a Simulation Platform for Multistage Stochastic Programming Problems. In April 2000, he joined the Foundation for Research on Information Technologies in Society (IT'IS) which had emerged from the former BIOEM/EMC group. There, he is involved in the development, optimization and dosimetric evaluation of exposure setups for bioexperiments within various studies related to the health risk assessment of mobile communications. He is also in charge of the development of a simulation platform optimized for antennas in complex environments, numerical dosimetry and optical devices.

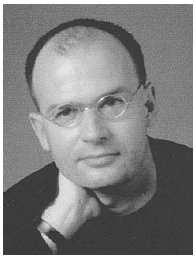

Niels Kuster was born 1957 in Olten, Switzerland, received the M.S. and Ph.D. degrees in Electrical Engineering from the Swiss Federal Institute of Technology (ETH) in Zürich. In 1993, he was elected Professor at the Department of Electrical Engineering of the Swiss Federal Institute of Technology (ETH) in Zürich, Switzerland. In 1992 he was Invited Professor at the Electromagnetics Laboratory of Motorola Inc. in Florida, USA and in 1998 at the Metropolitan University of Tokyo, Japan. In 1999 he was appointed as Director of the Foundation for Research on Information Technologies in Society, Switzerland. His research interest is currently focused on the area of reliable on/in-body wireless communications and related topics. This includes 1) measurement technology and 2) computational electrodynamics for evaluation of close near-fields in complex environments, 3) safe and reliable wireless communication links within the body or between implanted devices and the outside for biometrics applications; 4) development of exposure setups and quality control for bioexperiments evaluating interaction mechanisms, therapeutic effects as well as potential health risks; and 5) exposure assessments.